Published in final edited form as:
Nat Med. 2012 October ; 18(10): 1539–1549. doi:10.1038/nm.2899.

MitoNEET, a key regulator of mitochondrial function and lipid homeostasis

Christine M. Kusminski[1], **William L. Holland**[1], **Kai Sun**[1], **Jiyoung Park**[1], **Stephen B. Spurgin**[1], **Ying Lin**[2], **G. Roger Askew**[3], **Judith A. Simcox**[4], **Don A. McClain**[4,5], **Cai Li**[3], and **Philipp E. Scherer**[1,6,*]

[1]Touchstone Diabetes Center, Department of Internal Medicine, The University of Texas Southwestern Medical Center, Dallas, Texas 75390-8549

[2]Department of Cell Biology, Albert Einstein College of Medicine, Bronx, NY, 10461

[3]Department of Metabolic Disorders, Merck Research Laboratories, Rahway, NJ 07065

[4]Department of Medicine and Biochemistry, University of Utah School of Medicine, Salt Lake City, Utah

[5]Research Service, VA Medical Center, Salt Lake City, Utah

[6]Department of Cell Biology, The University of Texas Southwestern Medical Center, Dallas, Texas 75390-8549

Abstract

We examined rodent models with altered levels of mitoNEET, a protein residing in the mitochondrial outer membrane. Adipocyte-specific overexpression of mitoNEET enhances lipid-uptake and storage, leading to an expansion of adipose tissue mass. Despite the resulting massive obesity, benign aspects of adipose tissue expansion prevail and insulin sensitivity is preserved. MitoNEET inhibits mitochondrial iron transport into the matrix. Since iron is a rate-limiting component for electron transport, mitoNEET reduces β-oxidation rates. This is associated with reduced mitochondrial membrane potential and reduced reactive oxygen species damage, along with higher levels of adiponectin production. Conversely, the reduction of mitoNEET enhances mitochondrial respiratory capacity through enhanced iron content in the matrix, with reduced weight gain on a high fat diet. However, a reduction of mitoNEET also causes heightened oxidative-stress and glucose-intolerance. MitoNEET is therefore a potent regulator of mitochondrial function that profoundly impacts the dynamics of cellular and whole-body lipid homeostasis.

*corresponding author: philipp.scherer@utsouthwestern.edu, Telephone: (214) 648-8715, Fax: (214) 648-8720.

The microarray data has been uploaded to the Geo Database and can be accessed at http://www.ncbi.nlm.nih.gov/geo/query/acc.cgi?acc=GSE39251

Author Contributions

C.M.K. conducted all experiments and wrote the manuscript, except the portions indicated below.
W.L.H. helped with the ^{3}H-triolein uptake and β-oxidation experiments and performed the analyses.
K.S. generated TRE-mitoNEET mice.
J.P. helped plan, perform injections and scan fat-pads in Ctl-AAV and AAV-mitoNEET experiments.
S.S. generated the AAV-mitoNEET construct.
Y.L. performed the $DiOC_6$ ΔΨm experiment using mitoNEET-transfected 3T3-L1 preadipocytes.
R.A. and C.L. coordinated the generation of shRNA-MitoN knockdown mice.
J.A.P. and D.A.M. measured heme iron and provided high-iron-diet fed and *Hfe*−/− liver tissues.
P.E.S. was involved in experimental design, experiments, data analysis, and interpretation, in addition to writing of the manuscript.

Over the past decade, efforts have focused on the connection between mitochondrial dysfunction and the etiology of obesity, insulin resistance and the progression of type 2 diabetes mellitus (T2DM)[1,2]. Numerous studies indicate that metabolic disorders are accompanied with reduced mitochondrial content, compromised mitochondrial respiratory capacity, heightened oxidative-stress and consequently, altered whole-body lipid- and glucose metabolism[3,4]. The mechanisms that prompt compromised mitochondrial activity in obesity-driven T2DM and how targeting these processes will improve metabolic profiles remain largely unknown. Novel preclinical models that elucidate a role of mitochondria in cellular homeostasis have the potential to shed new light on these questions and allow us to define improved therapeutic avenues.

Healthy adipose tissue (AT) expansion has potent anti-diabetic effects by providing a safe haven to neutralize and store excess free fatty acids (FFAs). The inability to appropriately expand subcutaneous white adipose tissue (sWAT) may underlie the development of insulin resistance, β-cell failure and T2DM[5], by allowing the accumulation of lipid species that promote insulin resistance in cell-types vulnerable to lipotoxic effects. Adipocytes can also secrete adipokines that help buffer these lipotoxic side-effects of excess caloric-intake. A critical player in this area is adiponectin. Secreted exclusively from adipocytes, adiponectin promotes storage of triglycerides (TGs) preferentially in AT[5,6] to improve metabolic flexibility. Adiponectin further reduces the accumulation of ceramide species to improve cellular survival and insulin sensitivity. Mice overexpressing adiponectin in an *ob/ob* background exhibit improved insulin-sensitivity and lipid profiles[5]; such characteristics are attributed to augmented ceramidase activity[7], a redistribution of lipids and increased adipogenesis, concomitant with gross sWAT expansion. However, the underlying mechanisms that initiate this paradoxical phenomenon of lipid-redistribution and chronic AT expansion, to improve metabolic stature, are not fully defined.

Mitochondria play a central role in energy homeostasis by partitioning fuels toward β-oxidation or storage as fat. During AT expansion, the oxidation of lipid and carbohydrate fuels requires coordinated regulation of downstream metabolic pathways, such as the tricarboxylic acid cycle and the electron transport chain (ETC). Compromised mitochondrial energy production is a major anomaly in obesity. In particular, obese and type 2 diabetic subjects are known to exhibit lower β-oxidation rates, reduced oxidative enzymatic activities and decreased ETC activity[8,9]; concomitant with greater glycolytic capacities and increases in cellular fatty acid (FA)-uptake[10]. While these observations highlight oxidative failure during lipid accumulation, the mechanisms by which diminished β-oxidation and suboptimal mitochondrial function stimulate lipid-uptake and accumulation within obesity, have not been fully established.

Here, we take advantage of the unique properties of the mitochondrial membrane protein mitoNEET. Using gain and loss of function models for mitoNEET, we induce chronic and massive AT expansion, at least in part through an upregulation of adiponectin production and release from adipocytes. MitoNEET achieves these effects through a selective modulation of the mitochondrial electron transport activity. This establishes a tight functional connection between mitoNEET, mitochondrial activity and adiponectin release. Originally, mitoNEET was identified as a unique dimeric mitochondrial membrane target crosslinked to the thiazolidinedione (TZD), pioglitazone[11,12]. Located in the outer mitochondrial membrane, mitoNEET was named according to its C-terminal amino acid sequence, Asn-Glu-Glu-Thr (NEET)[11]. Furthermore, oriented towards the cytoplasm, the CDGSH domain of mitoNEET can bind redox-active, pH-labile 2Fe-2S clusters[13–15]; with pioglitazone reported to stabilize the protein against 2Fe-2S cluster release[12].

MitoNEET achieves its remarkable effects on cellular and systemic metabolic homeostasis on the basis of acting as a powerful regulator of mitochondrial iron content. We have taken advantage of these properties to influence mitochondrial bioenergetics and metabolism in a tissue- and cell-type specific manner; this results in remarkable alterations in whole-body energy homeostasis and further, opens up new avenues for cell-specific manipulation of mitochondrial activity in any cell-type of choice.

Results

MitoNEET promotes gross AT expansion

Mice can be metabolically challenged either by introducing specific genetic mutations or by providing them with a high-fat diet (HFD). Examination of tissues from mice exposed to such challenges revealed that the levels of the mitochondrial protein mitoNEET are markedly lower in AT and the liver (Fig. 1a), indicating that altered mitoNEET levels may be a hallmark of metabolically challenged tissues.

To address more directly whether mitoNEET activity can play a pertinent role in AT function, we utilized the 5.4 kb aP2-promoter[16] to generate an adipose-specific transgenic mouse model of mitoNEET overexpression (MitoN-Tg mice) (Fig. 1b). This leads to the overexpression of mitoNEET within physiological range (approximately 5-fold in sWAT, with lower levels observed in other fat-pads). Importantly, expression of the transgene is limited to adipocytes and not observed in other cell-types (including macrophages) (data not shown).

To assess the extent to which mitoNEET action can impact AT expansion, we applied a more prolonged metabolic challenge. We wanted to test how maintaining mitoNEET at elevated levels during AT expansion affects the cellular physiology of a mouse with a diabetic phenotype. We therefore generated *ob/ob* mice in a FVB background harboring the adipose-specific mitoNEET overexpression cassette. Both male and female MitoN-Tg *ob/ob* mice gained substantially more body-weight than their *ob/ob* littermates (Fig. 1c); with the heaviest female MitoN-Tg *ob/ob* mouse reaching 129.5 g in body-weight (Fig. 1d). Despite their body-weight, male and female MitoN-Tg *ob/ob* mice preserve euglycemic blood glucose concentrations, while *ob/ob* counterparts display diabetic hyperglycemic levels (male *ob/ob* mice: 474 ± 26 mg dl^{-1}; male MitoN-Tg *ob/ob* mice: 111 ± 14 mg dl^{-1}; female *ob/ob* mice: 411 ± 19 mg dl^{-1}; female MitoN-Tg *ob/ob* mice: 123 ± 6 mg dl^{-1}: $P < 0.001$) (Fig. 1e). An oral glucose tolerance test (OGTT) on these morbidly obese transgenic mice revealed a profile comparable to fully glucose-tolerant WT mice, despite utilizing an oral glucose dose based on body-weight, i.e. transgenic mice receive a 3- to 4 times higher glucose load than WT mice (Fig. 1f). In hyperinsulinemic-euglycemic clamp studies, MitoN-Tg *ob/ob* mice required a significant increase in the glucose infusion rate, when compared when *ob/ob* mice ($P < 0.01$, $n = 5$) (Fig. 1g); implicating an improvement in whole-body insulin sensitivity. Hepatic insulin sensitivity is further enhanced in MitoN-Tg *ob/ob* mice, as demonstrated by a marked reduction in hepatic glucose output (Fig. 1g). In line with an improved carbohydrate metabolism, liver, AT and pancreatic histology are normalized in MitoN-Tg *ob/ob* mice; with negligible hepatic lipid accumulation (Fig. 1h). A normalization of adipocyte cell size is apparent, concomitant with limited sWAT immune-cell infiltration (Fig. 1h). Moreover, MitoN-Tg *ob/ob* mice retain the number and morphology of islets, comparable to a WT mouse; whereas diabetic *ob/ob* mice retain less than half the number of islets (WT: 32 ± 2 islets; *ob/ob*: 14 ± 6 islets; MitoN-Tg *ob/ob*: 38 ± 2 islets). Furthermore, a dramatic reduction in fibrosis is apparent in MitoN-Tg *ob/ob* mice, primarily evident in sWAT, as judged by the reduced Trichrome Stain (Fig. 1h).

Ceramides are a group of sphingolipids that are frequently associated with insulin resistance[17]; in light of this, MitoN-Tg *ob/ob* mice exhibit significantly lower hepatic ceramide levels, when compared with *ob/ob* mice ($P < 0.05$, $n = 4$) (Fig. 1i). Similarly diacylglycerols (DAGs), another class of lipids that, when elevated in the liver, have been implicated in reduced cellular insulin responses[18]. Interestingly, MitoN-Tg *ob/ob* mice harbor markedly lower hepatic DAG levels, when compared with *ob/ob* mice (*ob/ob*: 1644.9 ± 180.3 pmol mg^{-1}; MitoN-Tg *ob/ob*: 936.8 ± 97.5 pmol mg^{-1}, $P < 0.05$); further suggesting an improved hepatic lipid profile.

Following an oral gavage of 20% intralipid, we subsequently examined F2-isoprostane levels as a measure of ROS-driven lipid-peroxidation[19]. Interestingly, MitoN-Tg *ob/ob* sWAT harbors markedly fewer ROS-induced lipid-peroxidation products than *ob/ob* sWAT (Fig. 1j); demonstrating a paradoxical low degree of oxidative stress existing in a morbidly obese setting. Similar observations were made in MitoN-Tg mice exposed to HFD in the absence of the *ob/ob* mutation (data not shown). In addition to this, we can initiate similar fat-pad expansion by directly infecting sWAT with a mitoNEET-expressing AAV virus, which prompts a local three fold overexpression of mitoNEET, versus injection of a control virus into the collateral fad-pad (data not shown). Collectively, this indicates that mitoNEET can promote AT expansion under multiple different conditions with multiple different overexpression approaches.

MitoNEET causes enhanced lipid uptake and adiponectin levels

Younger mice carrying the mitoNEET transgene in a WT background that are maintained on a chow-diet, exhibit no considerable differences in body-weight or insulin-sensitivity, when compared with WT mice (data not shown). We proposed that an unchallenged setting would be an ideal condition to evaluate the MitoN-Tg sWAT gene expression profile in more detail, since we would not have the additional confounders of chronic obesity and insulin resistance that alter the microarray profile secondary to the initial transcriptional changes. Therefore, Supplementary Table 1 highlights the main transcriptional fingerprints substantially altered in sWAT by mitoNEET overexpression. Gene regulatory pathways markedly altered in response to mitoNEET induction are adipogenesis, TG synthesis, NEFA re-esterification, FA biosynthesis, lipid-droplet associated protein synthesis, FA-uptake, FA-transport and glucose-uptake (Supplementary Table 1); these changes were confirmed through RT-PCR analysis (Fig. 2a and Supplementary Fig. 1). A list of RT-PCR primer sequences of differentially expressed genes identified by the microarray cluster analysis from sWAT derived from WT mice versus MitoN-Tg mice is highlighted in Supplementary Table 2. Interestingly, a marked upregulation in the FA transporter protein Cd36 suggested that mitoNEET action may alter the kinetics of cellular lipid uptake. Indeed, a triglyceride (TG) clearance test revealed a striking efficacy in the rate of lipid clearance in MitoN-Tg mice. While WT mice exhibit the expected hyperlipidemic excursion of TG upon exposure to an oral lipid gavage, MitoN-Tg mice display a significantly higher rate of TG clearance ($P < 0.01$, $P < 0.05$, $n = 6$) (Fig. 2b).

The ability of MitoN-Tg mice to rapidly dispose of exogenous lipids, coupled with the long term ability to enhanced fat mass expansion, is a phenotype reminiscent of adiponectin overexpressing mice[5]. The transcriptional upregulation of adiponectin that we observed in Figure 2a is consistent with a potential involvement of adiponectin in the process. Indeed, MitoN-Tg mice exhibit markedly higher circulating levels of adiponectin (Supplementary Table 3), with a prominent increase in the high-molecular weight form (data not shown); highlighting the ability of mitoNEET to exert a constitutive stimulatory effect on adiponectin production and release. The marked upregulation of adiponectin protein levels (Fig. 2c) are only evident in transgenic sWAT and not apparent in gWAT, suggesting local mitoNEET levels within a fat-pad govern adiponectin production. Indeed, adiponectin is

dose-dependently upregulated as a function of how much mitoNEET is expressed within a given fat-pad (Fig. 2d). In light of this tight correlation, we examined whether the mitoNEET-enhanced lipid clearance is mediated directly through adiponectin upregulation. MitoN-Tg adiponectin-knockout (MitoN-Tg *Adn*-KO) mice exhibit significantly lower rates of TG clearance, when compared with MitoN-Tg mice ($P < 0.05$, $n = 6$) (Fig. 2e); suggesting that augmented lipid-uptake at least partially, is dependent on a mitoNEET-adiponectin axis.

Whereas no differences are apparent between WT mice and MitoN-Tg mice in terms of systemic glucose and insulin levels under chow-fed conditions (Supplementary Table 3), we did however observe elevated systemic FFA and glycerol levels in MitoN-Tg mice upon fasting the mice for 24 hours (Supplementary Table 3); suggesting mitoNEET levels in adipocytes may influence fasting-induced lipolysis. In response to extracellular stimuli by catecholamines, adipocytes hydrolyze stored neutral TGs to liberate FFAs and glycerol[20]. Interestingly, following β-3 adrenergic agonist stimulation, MitoN-Tg mice exhibit considerably higher levels of glycerol release (Fig. 2f); a phenotype again similar to adiponectin transgenic mice[21]. However, FFA release is massively substoichiometric to glycerol release; while we expected theoretically 3 moles of FFA released for every glycerol molecule released (a number which is usually closer to a 2:1 ratio in WT mice), we observed less than 0.3 moles of FFAs liberated per mole of glycerol in the transgenics. This suggests that an extremely efficient re-esterification of FFAs to TG occurs, along with an excess local pool of glycerol. Such a phenomenon is particularly apparent in an *ob/ob* setting, whereby the profound reduction in FFA-efflux becomes problematic upon fasting; conditions under which glucose levels rapidly achieve hypoglycemic levels (data not shown). Pepck exerts a pertinent role in maintaining homeostasis of FFA re-esterification in AT[22], particularly through glyceroneogenesis[23]. The marked upregulation in Pepck message levels in MitoN-Tg sWAT (Supplementary Fig. 1) suggests a mitoNEET-induced Pepck-dependent stimulation of glyceroneogenic pathways, which may effectively promote FFA re-esterification into the TG pool within adipocytes. Finally, β-3 adrenergic stimulation of WAT is known to trigger rapid release of insulin[19]. We observed a sharp rise in insulin levels accompanied with severe hypoglycemia (data not shown), suggesting a fully functional and highly active adipo-insular axis in transgenic mice.

Lipoprotein lipase (Lpl) plays a key role in the clearance of circulating TGs and their routing toward storage or oxidative tissues. MitoN-Tg sWAT exhibits a significant increase in local Lpl activity in comparison to WT sWAT (WT sWAT: $14.6 \pm 3.5\ \mu U g^{-1}\ h^{-1}$; MitoN-Tg sWAT: $25.7 \pm 3.7\ \mu U g^{-1}\ h^{-1}$, $P < 0.001$), with no differences between gWAT fat-pads (Fig. 2g). These data indicate an exceptionally responsive subcutaneous fat-pad in transgenics; a phenotype critically dependent and directly proportional to the local overexpression of mitoNEET.

MitoNEET mediated effects on fatty acid metabolism

To further tie mitoNEET expression to fatty acid metabolism, we injected a ^{3}H-triolein tracer to gauge lipid-storage and β-oxidation rates. MitoN-Tg mice were shown to exhibit a significant 235% increase ($P < 0.001$) in the rate of whole-body ^{3}H-triolein clearance (Fig. 3a); with sWAT primarily responsible for the bulk of the differential (Fig. 3b), out of all the tissues examined (Supplementary Fig. 2a). Considering sWAT is the primary site of mitoNEET overexpression, the local increase in mitoNEET within subcutaneous adipocytes is likely to be the direct mediator of these effects on lipid clearance. In parallel, we noted markedly lower β-oxidation rates in MitoN-Tg sWAT and BAT (BAT being a secondary site of mitoNEET overexpression) (Fig. 3c and Supplementary Fig. 2b). Quantitatively, MitoN-Tg sWAT and BAT are substantially larger in size (Fig. 3d); consistent with a tight link to local overexpression of mitoNEET within these fat-pads. Visually, MitoN-Tg sWAT

appears darker in color in comparison to WT sWAT (Fig. 3e). Conversely, and presumably compensatory to sWAT hyperproliferation, MitoN-Tg gonadal WAT (gWAT) and mesenteric WAT (mWAT) fat-pads are markedly smaller in size when compared with WT gWAT and WT mWAT (Fig. 3d, 3e and Supplementary Fig. 2c). These observations suggest that by manipulating mitoNEET levels in different fat-pads differentially, we can disrupt the steady state distribution of lipid storage; thereby preferentially redistributing lipids towards fat-pads enriched in mitoNEET.

Qualitative histological examination of AT revealed smaller adipocyte-cell size in MitoN-Tg sWAT in comparison to WT sWAT (Fig. 3f); indicating that within a mitoNEET-enriched environment, healthy AT expansion through adipocyte hyperplasia prevails, rather than the metabolically unfavorable adipocyte hypertrophic expansion typically observed in states of obesity-associated insulin-resistance[24]. Finally, MitoN-Tg gWAT adipocytes are smaller in size when compared with WT gWAT adipocytes (Fig. 3f); suggesting a diversion of lipids away from this fat-pad to avoid hypertrophic adipocyte formation.

MitoNEET modulates mitochondrial function and iron content

Previous reports have established mitoNEET as an outer mitochondrial membrane protein. While the phenotypic changes associated with the alteration of mitoNEET levels are robust, the question arises as to how an outer mitochondrial membrane protein exerts such profound effects on β-oxidation rates. MitoNEET can serve as an iron-sulfur cluster transfer protein[25]; the physiological relevance of these clusters is however unknown; however they may play a role in mitochondrial iron metabolism. Indeed, we observe that mitoNEET overexpression at the level of the mitochondrion, brings adipocyte mitochondrial iron metabolism markedly out of balance. More specifically, MitoN-Tg sWAT mitochondria contain significantly lower levels of iron (Fig. 4a) ($P < 0.001$, $n = 7$). This reduction of mitochondrial iron by almost 50%, suggests a critical involvement of mitoNEET in supplying the components of the ETC with iron, a rate limiting component for ETC activity[26]. Furthermore, we noted markedly lower heme iron levels in MitoN-Tg sWAT mitochondria (data not shown); since mitochondrial heme synthesis and iron sulfur cluster metabolism are tightly linked processes[27], this further highlights mitoNEET-induced alterations in iron homeostasis. Moreover, when assessing either WT mice fed a high-iron diet, or mice with hemochromatosis (induced with a targeted deletion of the *Hfe* gene, which leads to defects in iron handling and a cellular iron overload)[28], we observe that *total* mitoNEET expression levels are considerably upregulated (Fig. 4b); with notable stabilization of a SDS-resistant mitoNEET *dimer* being apparent. This could be consistent with a counter-regulatory upregulation of mitoNEET under conditions of excess iron in an attempt to curb additional transport of iron into the mitochondrial matrix under conditions of iron overload.

To address how mitoNEET lowers β-oxidation and promotes lipid accumulation, we examined the adipocyte overexpression model further. When examining the mitochondrial membrane potential ($\Delta\Psi m$), 3T3-L1 preadipocytes stably transfected either with high or low concentrations of mitoNEET, exhibit low $\Delta\Psi m$ compared to controls (Fig. 4c); a similar degree of lowering occurs upon TZD treatment (Fig. 4c). Such a mitoNEET-induced reduction in $\Delta\Psi m$, may reflect either insufficient ETC activity[29], inefficient substrate supply to mitochondria, or an increased proton flux back into the mitochondrial matrix; all as a direct consequence of a local elevation in mitoNEET levels.

To directly establish whether mitoNEET alters ETC activity, we performed electron-flow (EF) analyses and assessed oxygen-consumption rates (OCRs); a method previously established to assess mitochondrial function[30]. Of note, such OCR measurements are performed in the presence of the chemical uncoupler, FCCP. MitoN-Tg sWAT mitochondria display markedly lower OCRs in response to the substrates pyruvate, malate, succinate and

ascorbate (Fig. 4d). Interestingly, MitoN-Tg sWAT mitochondria exhibit markedly higher OCRs in response to the complex I inhibitor, rotenone (Fig. 4d). Rotenone can promote ROS-induced oxidative-stress[31]; therefore an ineffective inhibition of complex I by rotenone in MitoN-Tg mitochondria suggests that an indirect interference by mitoNEET may minimize ROS-driven damage. Moreover, we observed that MitoN-Tg sWAT exhibits a significantly lower NAD^+/NADH ratio ($P < 0.001$, $n = 5$) (Fig. 4e). Such a build-up of reduced NADH equivalents in MitoN-Tg sWAT suggests that: i) NADH is insufficiently re-oxidized by the ETC or, mitoNEET may enhance glycolytic rates (an NADH-generating process) to compensate for reduced β-oxidation. Interestingly, in whole-tissue slices, in parallel with low OCRs in MitoN-Tg sWAT, we indeed observed a concomitant increase in glycolytic rates (as judged by a higher extracellular acidification rate ["ECAR"]; an established indicator of glycolysis[32]) (Supplementary Fig. 3). Such an increase in glycolytic flux supports a model of a mitoNEET-driven shift in substrate utilization and metabolism; from lipid-based substrates to carbohydrate-based substrates.

Defects in ETC activity profoundly impact ROS production[31,33]. Following an oral gavage of 20% intralipid to create an environment of heightened lipid-stimulated ROS-production within sWAT, we assessed F2-isoprostanes levels to gauge ROS-driven lipid-peroxidation[19]. Interestingly, MitoN-Tg sWAT harbors substantially fewer ROS-induced lipid-peroxidation products than WT sWAT (Fig. 4f). Low ROS concentrations in mitoNEET-enriched fat-pads are therefore a characteristic feature of mitoNEET overexpressing adipocytes. To complement these biochemical assays, we focused on mitochondrial morphology. EM analyses revealed that MitoN-Tg sWAT mitochondria are elongated and form long filamentous structures (Fig. 4g). Moreover, mitochondria are recurrently juxtaposed to lipid-droplet-like structures (Fig. 4g); a phenomenon observed in exercising skeletal-muscle mitochondria upon increasing energy demand[34]. More mitochondria are visible per AT section in MitoN-Tg sWAT (Fig. 4g), suggesting induction of mitochondrial biogenesis. The marked increase in peroxisome proliferator-activated-γ coactivator 1-α (Pgc1-α) message levels in MitoN-Tg sWAT (Fig. 2a), a key regulator of mitochondrial biogenesis[35], is consistent with this observation.

Liver-specific overexpression of mitoNEET

To examine an alternative, acute *in vivo* modality to induce mitoNEET overexpression in cells other than adipocytes, we generated a "TRE-mitoNEET mouse" (TRE-mitoN), in which the expression of mitoNEET is driven by a tetracycline-inducible promoter element (a *tet-responsive element* "TRE"). For this promoter to be operational, we require the presence of the "*tet-on*" transcription factor, rtTA. We provide this factor in a hepatocyte-specific fashion through a mouse that harbors the rtTA component under the control of a ubiquitously active Rosa26 promoter; however, a transcriptional stop cassette is inserted that is flanked by two *loxP* sites.

Upon exposure to an albumin promoter driven Cre recombinase, hepatocyte-specific, doxycycline (Dox)-inducible mitoNEET overexpression is achieved (Supplementary Fig. 4a). Following Dox-HFD feeding, we attain a substantial and reliable 3-fold overexpression in mitoNEET protein (Supplementary Fig. 4b). The purpose for this is that we can demonstrate the usefulness of mitoNEET as a manipulator of mitochondrial activity in other cell-types as well. Consistent with our model of mitoNEET overexpression in AT, a mitoNEET-driven augmentation in lipid storage is preserved in the liver. Qualitatively, hepatic lipid-droplets are more prevalent in TRE-mitoN mice when compared with WT mice (Supplementary Fig. 4c); this indeed reflects a decline in mitochondrial respiratory capacity (Supplementary Fig. 4d). Collectively, this suggests a similar effect exerted by mitoNEET in a cell-type distinct from adipocytes; indicating a common impact of mitoNEET on cellular physiology in different tissue types.

Diametrically opposed phenotype for mitoNEET loss of function

MitoNEET overexpression allowed us to effectively manipulate mitochondrial function. To examine whether we can manipulate mitochondrial activity in an opposite direction through mitoNEET reduction, we generated mice harboring a doxycycline-inducible shRNA-knockdown construct for mitoNEET (shRNA-mitoN mice) (Supplementary Fig. 5a); this construct is effective in a majority of tissues, including adipose tissue and the liver (data not shown), thus creating a systemic inducible knockdown of mitoNEET. Following Dox-chow diet feeding, we observed a marked reduction of mitoNEET protein in AT and liver (Supplementary Fig. 5b); the tissues we opted to primarily focus our analysis on. Initial observations revealed that during Dox-HFD feeding, shRNA-mitoN mice gain considerably less body-weight in comparison to WT littermates (Fig. 5a). Surprisingly, despite displaying lower body-weights, shRNA-mitoN mice exhibit worsened glucose-tolerance (Fig. 5b). Given that we effectively modulate the ETC with mitoNEET overexpression, we hypothesized that this deterioration in insulin-sensitivity may arise from an intensified level of oxidative-stress[33,36]. Indeed, shRNA-mitoN mice harbor a high degree of hepatic ROS-induced protein damage (Fig. 5c), as assessed by enhanced levels of protein carbonylation; methodology previously established to gauge oxidative damage within a cell[37]. Consistent with this, anti-oxidant treatment of WT and shRNA-mitoN MEFs or primary hepatocytes isolated from WT and knockdown animals could reverse a palmitate-induced reduction in phospho-Akt (p-Akt) levels (Supplementary Fig. 5c), suggests the ROS-associated worsening in glucose tolerance may be alleviated utilizing anti-oxidant treatments to reverse the negative impact on insulin signaling.

Histological examination of livers following Dox-HFD feeding revealed that shRNA-mitoN mice exhibit reduced lipid accumulation in comparison to WT livers (Fig. 5d); suggesting a local augmentation in β-oxidation. When examining $\Delta\Psi m$, we observed substantially enhanced tetramethylrhodamine methyl ester (TMRM) staining in Dox-induced shRNA-mitoN MEFs, compared with WT MEFs treated with or without Dox (Fig. 5e). In terms of mitochondrial oxidative capacity, shRNA-mitoN MEFs exhibit significantly higher OCRs in response to palmitate, when compared with WT MEFs ($P < 0.001$, $n = 10$) (Fig. 5f); directly demonstrating that a reduction in mitoNEET enhances β-oxidation. When assessing electron flow (EF), hepatic mitochondria isolated from Dox-chow-fed shRNA-mitoN mice display markedly higher OCRs in response to pyruvate, malate, succinate and ascorbate (Fig. 5g); indicating higher mitochondrial activity in the absence of mitoNEET, regardless of the substrate source in this case. In light of this, a previous report with a partial characterization of cardiac mitochondria isolated from a systemic constitutive mitoNEET-knockout mouse demonstrated reduced oxidative capacity[13]. It is unclear what leads to these differential effects; however, it is likely that tissues utilized in these latter studies that develop in the constitutive absence of mitoNEET may display compensatory mechanisms that prevail under the assay conditions employed. All the read-outs examined with our loss-of-function mice are diametrically opposed to the gain of function phenotypes in the first part of the analysis. This suggests that there may be a similar underlying mechanism that affects mitochondrial activity over the entire range of differential mitoNEET levels. Finally, we observed higher levels of mitochondrial iron with a reduction in mitoNEET (Fig. 5h); consistent with a role of mitoNEET as a key factor in the regulation of mitochondrial iron content.

Discussion

We have developed a novel tool to specifically alter the levels of mitochondrial activity in adipocytes and hepatocytes. We took advantage of the properties of the mitochondrial protein mitoNEET that allowed us to profoundly alter mitochondrial function and lipid homeostasis in a cell-type specific fashion, thereby altering whole-body insulin-sensitivity.

We observe these effects in a complimentary set of mouse models that involve multiple, independent approaches to achieve alterations in mitoNEET levels within a physiological range. We utilize an adipose-specific transgenic, an inducible tissue-specific overexpression system and an inducible constitutive knockdown of mitoNEET. The overexpression of mitoNEET allows us to compromise mitochondrial function to disrupt cellular energy balance; driving a decline in β-oxidation and causing a compensatory enhancement in cellular nutrient-uptake. This triggers chronic AT expansion and mice grow massively obese, on par with, or substantially higher than the maximum weight reported in the literature for *mus musculus*. Despite the obesity, mitoNEET overexpression during high caloric-intake results in insulin-sensitive mice, thereby providing a model of a "metabolically healthy, obese state" that minimizes lipotoxicity in tissues prone to store lipids during excess caloric-intake (Fig. 6); a phenomenon that is also observed clinically[38]. We focused our analysis primarily on AT, however an up-regulation and knockdown in mitoNEET causes profound mitochondrial alterations in hepatocytes, mouse embryonic and 3T3-L1 fibroblasts; suggesting that the observations in adipocytes may apply to other cell-types as well. Future assessments should reveal more systematically which cell-types are particularly prone to regulation by mitoNEET and, under what physiological conditions this regulation may be relevant. This may be a function of how much "spare capacity" mitochondria have under a given physiological condition, i.e. whether they operate at a near maximal rate (relative to the completely uncoupled state). Such mitochondria would be more dramatically affected by subtle changes in mitochondrial iron metabolism.

Ectopic lipid accumulation is a major risk factor in the progression of insulin resistance[39]. Our adipocyte-specific overexpressors have only minimal levels of ectopic lipids, thereby preserving insulin sensitivity despite excess caloric-intake. The mechanisms for partitioning lipid storage *versus* β-oxidation are not fully defined, particularly in the context of the adipocyte. A key phenotype in transgenic mice is their enhanced lipid-uptake and storage into sWAT; suggesting that mitoNEET may contribute to adjusting the relative ratio of energy stored *versus* energy burnt by altering mitochondrial bioenergetics. Another key finding is that manipulation of β-oxidation at the level of the white adipocyte causes a profound net systemic contribution towards whole-body energy homeostasis. In our model, "backed-up" β-oxidation may increase the cellular pool of Ppar-γ ligands; both high Ppar-γ levels and increased adipogenesis in the transgenic setting are consistent with this.

Adiponectin is a 30 kDa protein secreted exclusively from adipocytes that exerts anti-diabetic, anti-inflammatory and anti-atherogenic properties[6,7]. Adequate mitochondrial function and biogenesis are critical determinants for the folding and secretion of adiponectin[40–42]; therefore, one of our aims was to establish and strengthen this relationship further. Indeed, mitoNEET overexpression causes a substantial increase in adiponectin levels, both transcriptionally and post-transcriptionally in transgenic sWAT; prompting an increase in circulating levels. This upregulation of adiponectin may also be central to the enhanced TG-clearance in mitoNEET transgenic mice; since this effect is blunted when we cross mitoNEET-overexpressing mice into an adiponectin-null background. Taken together, the adipocyte-specific impairment in β-oxidation leads to a dramatic local increase in adiponectin production and release; this may be a valuable observation in the context of our teleological understanding of the function of adiponectin, which may serve to gauge the mitochondrial lipid demand in adipocytes. Adiponectin could therefore act as a powerful systemic signal to drive dietary and tissue lipids towards the adipocyte[5]. Future studies will however need to delineate the detailed mechanistic steps that connect compromised mitochondrial function with the paradoxical *increase* in adipocyte-derived adiponectin production.

The mitochondrial membrane potential ($\Delta\Psi m$) is a critical parameter that reflects ETC activity. Considerable loss or depolarization of $\Delta\Psi m$ could lead to low cellular energy levels[43]; as cells with impaired OXPHOS exhibit low $\Delta\Psi m$[44]. Overexpressing mitoNEET in 3T3-L1 preadipocytes lowers $\Delta\Psi m$, indicating some degree of energy depletion. Therefore, either over-abundance of mitoNEET (compromising mitochondrial function) or a reduction in mitoNEET (potential for rapid cellular substrate depletion due to excessive mitochondrial activity), may bring mitochondrial function out of sync with cellular energy requirements; accentuating that the levels of mitoNEET must be harmonized with intracellular energy demands. Alterations in mitoNEET further allow us to manipulate ROS levels. Heightened ROS generation results from severe alterations in oxidative metabolism[31]. While ROS levels intensify with obesity[45], a mitoNEET-induced increase in lipid-uptake, accompanied with low β-oxidation, may alleviate the burden of flux through ROS producing β-oxidation pathways, thereby protecting AT from ROS-induced oxidative injury. This paradox of low ROS generation in an oversized, lipid-laden fat-pad implies a fully functional ROS-scavenging system. No mitochondrial dysfunction *per se* exists in a mitoNEET-enriched environment, rather an insufficient rate in ETC activity. Interestingly, ROS generation is greater when basal respiration is supported by FAs, rather than by carbohydrate-based substrates[46]. Low β-oxidation rates accompanied by high glycolytic rates upon mitoNEET overexpression may further sustain low ROS production. Oxidative-stress is also a robust negative correlate of insulin-sensitivity[33,36,47]. Despite gaining less body-weight during HFD-feeding, mitoNEET knockdown mice exhibit high ROS-induced protein damage and are less glucose-tolerant. ROS generation is prominent when the proton motive force (pmf) is large[48]; for instance hyperglycemia-induced hyperpolarization elevates ROS production, owing to enhanced cellular respiration[49]. The high $\Delta\Psi m$ following mitoNEET reduction, accompanied with enhanced oxygen-consumption rates, implicates that ROS may contribute to the glucose-intolerance. Indeed, other mouse models engineered to *increase* flux through β-oxidation pathways develop severe insulin resistance, despite harboring protection from HFD-induced obesity[50]. Our *in vitro* results in this system indeed confirm that anti-oxidant treatment of cells harboring decreased mitoNEET levels, leads to improvements in cellular insulin signal transduction.

Two key regulators of ETC activity and ROS concentrations are the intracellular redox-potential of NAD^+/NADH and the pmf. A surplus of reduced equivalents, NADH and $FADH_2$, formed through glycolysis and the TCA cycle, are re-oxidized through the ETC. *Vice versa*, a mismatch between β-oxidation and ETC activity disrupts the energy milieu of mitochondria by perturbing redox status[1] to reduce the NAD^+/NADH ratio. As mitoNEET lowers the NAD^+/NADH ratio, the build-up of NADH implies that: i) compensatory high glycolytic rates may generate surplus NADH from the decline in β-oxidation, ii) ETC activity is insufficient to re-oxidize NADH, iii) mitoNEET may impact NAD/NADH flux through various catabolic pathways, or iv) mitoNEET may alter NAD shuttle systems, salvage or degradation, such that mitochondrial performance is further perturbed by rising NADH concentrations[1].

Low mitochondrial iron content can decrease the activity of iron-containing ETC complexes and enzymes to diminish respiratory activity[26]. An excess of mitoNEET causes reduced levels of mitochondrial iron, and *vice versa*, a reduction of mitoNEET causes an increase in iron and ETC activity. This pinpoints iron transport as one of the critical aspects of mitoNEET function. In fact, Huang and colleagues recently demonstrated that iron overload (in the context of hereditary hemochromatosis) is associated with a shift from glucose to fatty acid oxidation and an increased risk for the development of diabetes[28]. These observations are fully consistent with the findings reported here; where a downregulation of mitoNEET leads to similar phenotypic manifestations.

In summary, we identify the mitochondrial protein mitoNEET as valuable tool in energy homeostasis and lipid metabolism. We utilize mitoNEET as a genetic tool to manipulate ETC activity by taking advantage of its ability to exert control over mitochondrial iron availability. We demonstrate that within the adipocyte, mitoNEET compromises mitochondrial efficacy, triggers a massive nutrient influx into the cell, enhances adiponectin production and increases β-adrenergic sensitivity. The increased lipid influx, combined with reduced oxidative capacity initiates massive AT expansion; despite obesity, insulin-sensitivity is preserved. Several of these effects are likely dependent on a mitoNEET-mediated adiponectin induction. Such mitoNEET-driven alterations in mitochondrial function therefore represent pivotal mechanisms that link obesity-related insulin resistance with mitochondrial perturbations and further, open the door to effective manipulation of mitochondrial activity in additional cell-types.

Methods

Animals

All animal experimental protocols were approved by the Institutional Animal Care and Use Committee of University of Texas Southwestern Medical Center at Dallas. Adipose-specific mitoNEET transgenic mice were generated by subcloning the mitoNEET gene into a plasmid containing the 5.4 kb aP2-promoter and a conventional 3' untranslated region[5]. Following linearization, the construct was injected into FVB-derived blastocysts. Transgene-positive offspring were genotyped using PCR with the primer set: 5'-GGACCTCTGATCATCAAGA-3' and 5'-GGAGACAATGGTTGTCAAC-3'. All overexpression experiments were performed in a pure FVB background. Adiponectin null mice were previously described[51]. Generation of doxycycline-inducible shRNA-mitoN knockdown and mitoNEET overexpression mouse models are detailed in the **Supplementary Methods**. All experiments were conducted using littermate-controlled male or female mice. All HFD experiments were initiated at 6–12 weeks of age. Mice were fed either standard-chow diet (No. 5058, LabDiet), a Dox-chow diet (600 mg kg^{-1} Dox; Bio-Serv), a 60% HFD (D12492, Research Diets Inc.) or a Dox-HFD (600 mg kg^{-1} Dox; Bio-Serv).

Systemic tests

For OGTTs, mice were fasted for 3 h prior to administration of glucose (2.5 g kg^{-1} body-weight by gastric gavage). Glucose levels were measured using an oxidase-peroxidase assay (Sigma-Aldrich). For TG clearance, mice were fasted (16 h), then gavaged 15 ul g^{-1} body-weight of 20% intralipid (Fresenius Kabi Clyton, L.P.). Blood was collected at timed intervals then assayed for TG levels (Infinity; Thermo Fisher Scientific) and FFA levels (NEFA-HR(2); Wako Pure Chemical Industries). For β_3-adrenergic receptor-agonist tests, blood samples were obtained before and 5-, 15- and 60 min following intraperitoneal injection of 1 mg kg^{-1} CL 316,243 (Sigma-Aldrich). Insulin and adiponectin levels were measured using commercial ELISA kits (Millipore Linco Research). Glycerol and glucose levels were determined using a free glycerol reagent and an oxidase-peroxidase assay, respectively (Sigma-Aldrich).

Hyperinsulinemic-euglycemic clamps

Hyperinsulinemic-euglycemic clamps were performed on conscious, unrestrained 10-week old male FVB *ob/ob* and MitoN-Tg *ob/ob* mice, as previously described[7,52].

Quantitative RT-PCR and microarray

Tissues were excised from mice and snap-frozen. Total RNA was isolated following tissue homogenization in Trizol (Invitrogen), then isolated using an RNeasy RNA extraction kit (Qiagen). cDNA was prepared by reverse transcribing 1 ug of RNA with SuperScript III reverse transcriptase and oligo$(dT)_{20}$ (Invitrogen). Supplementary Table 2 highlights the primer sets utilized for quantitative RT-PCR. Results were calculated using the threshold cycle method[53], with β-actin for normalization. For microarray, total cDNA was synthesized from sWAT, then spotted onto a mouse Illumina BeadArray platform (Illumina, Inc.). Fold-change and significance were calculated based on three independent replicates. Gene lists and cluster analyses of the data sets were performed using Ingenuity software (Ingenuity Systems Inc.).

Immunoblotting

Frozen tissue was homogenized in TNET buffer (50 mM Tris-HCl [pH 7.6], 150 mM NaCl, 5 mM EDTA, phosphatase inhibitors (Sigma Aldrich) and protease inhibitors (Roche)), then centrifuged to removal any adipose-layer present. Following Triton X-100 addition (final concentration of 1%), protein concentrations were determined using a bicinchoninic acid assay (BCA) kit (Pierce). Proteins were resolved on 4–12% bis-Tris gels (Invitrogen) or 10–20% Tricine gels (Invitrogen) then transferred to polyvinylidene difluoride membranes (Millipore) or nitrocellulose membranes (Protran, Whatman GmbH), respectively. A rabbit polyclonal antibody was raised against mouse mitoNEET with purified protein of a carboxy-terminal fusion of full-length murine mitoNEET to glutathione S-transferase (1:1000). Anti-adiponectin antibodies (1:1000) were utilized, as previously described[54]. Phospho-Akt (Ser473, #4060) and total-Akt (#2920) (Cell Signaling Technology, Inc.) were used (1:1000) for insulin signaling studies. Primary antibodies were detected using secondary immunoglobulin Gs labeled with infrared dyes emitting at 700 nm (926–32220) or 800 nm (926–32211) (both at 1:5000 dilutions) (Li-Cor Bioscience) then visualized on a Li-Cor Odyssey infrared scanner (Li-Cor Bioscience). The scanned data were analyzed using Odyssey Version 2.1 software (Li-Cor Bioscience). The complex distribution of adiponectin was determined as previously described[5]. Tissue Lpl activity was determined as previously detailed[55]. NAD^+ and NADH levels were assessed according to manufacturers' instructions (BioVision Inc.). Iron content was measured using commercial kits (BioAssay Systems). Hepatic ceramide and hepatic diacylglycerol levels were determined as previously detailed[7].

Histology and immunohistochemistry

Fat-pads or liver tissues were excised and fixed in 10% PBS-buffered formalin for 24 h. Following paraffin embedding and sectioning (5 μm), tissues were stained with H&E or a Masson's Trichrome stain. For immunohistochemistry, paraffin-embedded sections were stained using monoclonal anti-Mac2 antibodies (1:1000) (#CL8942AP, CEDARLANE Laboratories USA Inc.).

Preparation of mouse embryonic fibroblasts (MEFs) and isolation of mitochondria

MEFs were derived from WT or shRNA-mitoN E13.5 embryos with a C57BL/6J background. MEFs were cultured in DMEM containing glutamine, nonessential amino acids, penicillin/streptomycin, 20 mM HEPES and 10% FBS at 37 °C under 5% CO_2. For insulin signaling studies, WT and shRNA-mitoN MEFs were cultured in Dox-containing DMEM (1 μg ml^{-1}), then treated with either palmitate (400 μM; Sigma-Aldrich) or MnTBAP (1 mg ml^{-1}; Cayman Chemical Company) for 4 h. Cells were then acutely treated with insulin (16 nM; Sigma-Aldrich) for 10 min prior to cell harvesting and protein extraction for Western blot analysis. To isolate mitochondria, fresh tissues were homogenized using a drill-operated Teflon pestle in ice-cold MSHE buffer (70 mM sucrose,

210 mM mannitol, 5 mM HEPES, 1 mM EDTA) containing either 4% FA-free BSA (for AT) or 0.5% FA-free BSA (for liver). Following low centrifugation (800 g for 10 min), then high centrifugation (8,000 g for 10 min), the mitochondrial pellet was resuspended in the corresponding MSHE buffer and protein concentrations were determined using a BCA kit (Pierce).

Mitochondrial experiments

OCR and ECAR values were determined using the XF24 Extracellular Flux Analyzer (Seahorse Bioscience) following the manufacturers' protocols. For β-oxidation, WT MEFs and shRNA-mitoN MEFs (60,000 per well; 1 μg ml^{-1} Dox) were seeded overnight in a XF24 cell-culture microplate at 37 °C under 5% CO_2 (Seahorse Bioscience). Following 1 hr equilibration with 1X KHB buffer (111 mM NaCl, 4.7 mM KCl, 2 mM $MgSO_4$, 1.2 mM Na_2HPO_4) supplemented with 0.5 mM carnitine and 2.5 mM glucose, cells were subjected to treatment of a palmitate-BSA-conjugate (200 μM; C:16:0), followed by etomoxir (100 μM). OCR measurements were recorded at set interval time-points. For electron-flow (EF) measurements, isolated mitochondria were pelleted in a XF24 cell-culture microplate by centrifugation (2,000 g for 20 min at 4 °C) in 1X MAS buffer (70 mM sucrose, 220 mM mannitol, 10 mM KH_2PO_4, 5 mM $MgCl_2$, 2 mM HEPES, 1 mM EDTA in 0.2% FA-free BSA) supplemented with 10 mM pyruvate, 10 mM malate and 4 μM FCCP. OCR and ECAR measurements were obtained following sequential additions of rotenone (2 μM final concentration), succinate (10 mM), antimycin A (4 μM) and ascorbate (10 mM) (the latter containing 1 mM TMPD). For ECAR glycolytic flux experiments using whole-tissue slices, oligomycin (2 μM), FCCP (4 μM), 2-DG (100 mM) and antimycin A (10 μM) were added to tissues in an XF24 islet-capture Microplate (Seahorse Bioscience). All compounds and materials above were obtained from Sigma-Aldrich. For mitochondrial oxidative-stress, the protein-carbonylation assay was performed as previously described[37]. For lipid-peroxidation, bound 8-isoPGF2α levels were determined as previously detailed[19]. The mitochondrial membrane potential ($\Delta\Psi m$) experiments are detailed in the Supplementary Methods.

^{3}H-triolein uptake and β-oxidation

For measurements of endogenous triolein clearance rates, tissue-specific lipid-uptake and β-oxidation rates in transgenic tissues, methodologies were adapted from previously detailed studies[56,57]. Briefly, ^{3}H-triolein was tail-vein injected (2 μCi/mouse in 100 ul of 5% intralipid) into mice following a 16 h fast. Briefly, blood samples (0.15 ml) were then collected at 1, 2, 5, 10 and 15 min post injection. After 20 min following injection, mice were sacrificed, blood samples were taken and tissues were quickly excised, weighed and frozen at –80 °C until processing. Lipids were then extracted using a chloroform-to-methanol based extraction method[58]. The radioactivity content of tissues, including blood samples, was quantified as described previously[57].

Statistics

All results are provided as means ± standard errors of the mean. All statistical analysis was performed using GraphPad Prism. Differences between the two groups over time (indicated in the relevant figure legends) were determined by a two-way analysis of variance (ANOVA) for repeated measures. For comparison between two independent groups, a Student's *t* test was utilized. Significance was accepted at a *P* value of <0.05.

Supplementary Material

Refer to Web version on PubMed Central for supplementary material.

Acknowledgments

We kindly thank P.D. Neufer, G. Schatz and C.B. Newgard for helpful comments and suggestions. We would also like to thank J. Song and J. Xia for technical assistance, in addition to the rest of the Scherer laboratory, R. Unger and D. Clegg for helpful discussions. We would also like to thank P. Blanchard and Y. Deshaies for kindly providing LPL activity measurements, R. Hammer and the UTSW Transgenic Core Facility for the generation of mouse models as well as the UTSW Metabolic Core Facility for help in the phenotypic characterization of the mice and G. Milne from Vanderbilt University Medical Center for F2-isoprostane analysis. The authors were supported by US National Institutes of Health grants R01-DK55758, RC1-DK086629 and P01-DK088761 (P.E.S.), K99-DK094973 and an AHA Beginning Grant in Aid 12BGI-A8910006 (W.L.H.), R01-DK081842 (D.A.M.), T32-DK091317 (J.A.S.) and Department of Defense Fellowship USAMRMC-BC085909 (J.P.). C.M.K. was supported by a fellowship from the Juvenile Diabetes Foundation (JDRF 3-2008-130).

References

1. Muoio DM, Newgard CB. Obesity-related derangements in metabolic regulation. Annu Rev Biochem. 2006; 75:367–401. [PubMed: 16756496]
2. Lowell BB, Shulman GI. Mitochondrial dysfunction and type 2 diabetes. Science. 2005; 307:384–387. [PubMed: 15662004]
3. Mehta JL, Rasouli N, Sinha AK, Molavi B. Oxidative stress in diabetes: a mechanistic overview of its effects on atherogenesis and myocardial dysfunction. Int J Biochem Cell Biol. 2006; 38:794–803. [PubMed: 16442834]
4. Morino K, Petersen KF, Shulman GI. Molecular mechanisms of insulin resistance in humans and their potential links with mitochondrial dysfunction. Diabetes. 2006; 2(55 Suppl):S9–S15. [PubMed: 17130651]
5. Kim JY, et al. Obesity-associated improvements in metabolic profile through expansion of adipose tissue. J Clin Invest. 2007; 117:2621–2637. [PubMed: 17717599]
6. Scherer PE, Williams S, Fogliano M, Baldini G, Lodish HF. A novel serum protein similar to C1q, produced exclusively in adipocytes. J Biol Chem. 1995; 270:26746–26749. [PubMed: 7592907]
7. Holland WL, et al. Receptor-mediated activation of ceramidase activity initiates the pleiotropic actions of adiponectin. Nat Med. 17:55–63. [PubMed: 21186369]
8. Kelley DE, He J, Menshikova EV, Ritov VB. Dysfunction of mitochondria in human skeletal muscle in type 2 diabetes. Diabetes. 2002; 51:2944–2950. [PubMed: 12351431]
9. Ritov VB, et al. Deficiency of subsarcolemmal mitochondria in obesity and type 2 diabetes. Diabetes. 2005; 54:8–14. [PubMed: 15616005]
10. Simoneau JA, Veerkamp JH, Turcotte LP, Kelley DE. Markers of capacity to utilize fatty acids in human skeletal muscle: relation to insulin resistance and obesity and effects of weight loss. FASEB J. 1999; 13:2051–2060. [PubMed: 10544188]
11. Colca JR, et al. Identification of a novel mitochondrial protein (“mitoNEET”) cross-linked specifically by a thiazolidinedione photoprobe. Am J Physiol Endocrinol Metab. 2004; 286:E252–E260. [PubMed: 14570702]
12. Paddock ML, et al. MitoNEET is a uniquely folded 2Fe 2S outer mitochondrial membrane protein stabilized by pioglitazone. Proc Natl Acad Sci U S A. 2007; 104:14342–14347. [PubMed: 17766440]
13. Wiley SE, Murphy AN, Ross SA, van der Geer P, Dixon JE. MitoNEET is an iron-containing outer mitochondrial membrane protein that regulates oxidative capacity. Proc Natl Acad Sci U S A. 2007; 104:5318–5323. [PubMed: 17376863]
14. Wiley SE, et al. The outer mitochondrial membrane protein mitoNEET contains a novel redox-active 2Fe-2S cluster. J Biol Chem. 2007; 282:23745–23749. [PubMed: 17584744]
15. Lin J, Zhou T, Ye K, Wang J. Crystal structure of human mitoNEET reveals distinct groups of iron sulfur proteins. Proc Natl Acad Sci U S A. 2007; 104:14640–14645. [PubMed: 17766439]
16. Graves RA, Tontonoz P, Platt KA, Ross SR, Spiegelman BM. Identification of a fat cell enhancer: analysis of requirements for adipose tissue-specific gene expression. J Cell Biochem. 1992; 49:219–224. [PubMed: 1644859]
17. Chavez JA, Summers SA. A ceramide-centric view of insulin resistance. Cell Metab. 15:585–594. [PubMed: 22560211]

18. Jornayvaz FR, Shulman GI. Diacylglycerol activation of protein kinase cepsilon and hepatic insulin resistance. Cell Metab. 15:574–584. [PubMed: 22560210]
19. Milne GL, Sanchez SC, Musiek ES, Morrow JD. Quantification of F2-isoprostanes as a biomarker of oxidative stress. Nat Protoc. 2007; 2:221–226. [PubMed: 17401357]
20. Langin D. Adipose tissue lipolysis as a metabolic pathway to define pharmacological strategies against obesity and the metabolic syndrome. Pharmacol Res. 2006; 53:482–491. [PubMed: 16644234]
21. Asterholm IW, Scherer PE. Enhanced metabolic flexibility associated with elevated adiponectin levels. Am J Pathol. 176:1364–1376. [PubMed: 20093494]
22. Franckhauser S, et al. Increased fatty acid re-esterification by PEPCK overexpression in adipose tissue leads to obesity without insulin resistance. Diabetes. 2002; 51:624–630. [PubMed: 11872659]
23. Hanson RW, Reshef L. Glyceroneogenesis revisited. Biochimie. 2003; 85:1199–1205. [PubMed: 14739071]
24. Sun K, Kusminski CM, Scherer PE. Adipose tissue remodeling and obesity. J Clin Invest. 121:2094–2101. [PubMed: 21633177]
25. Zuris JA, et al. Facile transfer of [2Fe-2S] clusters from the diabetes drug target mitoNEET to an apo-acceptor protein. Proc Natl Acad Sci U S A. 108:13047–13052. [PubMed: 21788481]
26. Macdonald VW, Charache S, Hathaway PJ. Iron deficiency anemia: mitochondrial alpha-glycerophosphate dehydrogenase in guinea pig skeletal muscle. J Lab Clin Med. 1985; 105:11–18. [PubMed: 2981941]
27. Crooks DR, Ghosh MC, Haller RG, Tong WH, Rouault TA. Posttranslational stability of the heme biosynthetic enzyme ferrochelatase is dependent on iron availability and intact iron-sulfur cluster assembly machinery. Blood. 115:860–869. [PubMed: 19965627]
28. Huang J, et al. Iron overload and diabetes risk: a shift from glucose to Fatty Acid oxidation and increased hepatic glucose production in a mouse model of hereditary hemochromatosis. Diabetes. 60:80–87. [PubMed: 20876715]
29. Mitchell P. Keilin's respiratory chain concept and its chemiosmotic consequences. Science. 1979; 206:1148–1159. [PubMed: 388618]
30. Rogers GW, et al. High throughput microplate respiratory measurements using minimal quantities of isolated mitochondria. PLoS One. 6:e21746. [PubMed: 21799747]
31. Rigoulet M, Yoboue ED, Devin A. Mitochondrial ROS generation and its regulation: mechanisms involved in H(2)O(2) signaling. Antioxid Redox Signal. 14:459–468. [PubMed: 20649461]
32. Wu M, et al. Multiparameter metabolic analysis reveals a close link between attenuated mitochondrial bioenergetic function and enhanced glycolysis dependency in human tumor cells. Am J Physiol Cell Physiol. 2007; 292:C125–C136. [PubMed: 16971499]
33. Houstis N, Rosen ED, Lander ES. Reactive oxygen species have a causal role in multiple forms of insulin resistance. Nature. 2006; 440:944–948. [PubMed: 16612386]
34. Tarnopolsky MA, et al. Influence of endurance exercise training and sex on intramyocellular lipid and mitochondrial ultrastructure, substrate use, and mitochondrial enzyme activity. Am J Physiol Regul Integr Comp Physiol. 2007; 292:R1271–R1278. [PubMed: 17095651]
35. Lin J, Puigserver P, Donovan J, Tarr P, Spiegelman BM. Peroxisome proliferator-activated receptor gamma coactivator 1beta (PGC-1beta), a novel PGC-1-related transcription coactivator associated with host cell factor. J Biol Chem. 2002; 277:1645–1648. [PubMed: 11733490]
36. Bonnard C, et al. Mitochondrial dysfunction results from oxidative stress in the skeletal muscle of diet-induced insulin-resistant mice. J Clin Invest. 2008; 118:789–800. [PubMed: 18188455]
37. Curtis JM, et al. Downregulation of adipose glutathione S-transferase A4 leads to increased protein carbonylation, oxidative stress, and mitochondrial dysfunction. Diabetes. 59:1132–1142. [PubMed: 20150287]
38. Karelis AD, et al. The metabolically healthy but obese individual presents a favorable inflammation profile. J Clin Endocrinol Metab. 2005; 90:4145–4150. [PubMed: 15855252]
39. McGarry JD. Banting lecture 2001: dysregulation of fatty acid metabolism in the etiology of type 2 diabetes. Diabetes. 2002; 51:7–18. [PubMed: 11756317]

40. Koh EH, et al. Essential role of mitochondrial function in adiponectin synthesis in adipocytes. Diabetes. 2007; 56:2973–2981. [PubMed: 17827403]
41. Frizzell N, et al. Succination of thiol groups in adipose tissue proteins in diabetes: succination inhibits polymerization and secretion of adiponectin. J Biol Chem. 2009; 284:25772–25781. [PubMed: 19592500]
42. Iwabu M, et al. Adiponectin and AdipoR1 regulate PGC-1alpha and mitochondria by Ca(2+) and AMPK/SIRT1. Nature. 464:1313–1319. [PubMed: 20357764]
43. Sherratt HS. Mitochondria: structure and function. Rev Neurol (Paris). 1991; 147:417–430. [PubMed: 1962047]
44. Dey R, Moraes CT. Lack of oxidative phosphorylation and low mitochondrial membrane potential decrease susceptibility to apoptosis and do not modulate the protective effect of Bcl-x(L) in osteosarcoma cells. J Biol Chem. 2000; 275:7087–7094. [PubMed: 10702275]
45. Furukawa S, et al. Increased oxidative stress in obesity and its impact on metabolic syndrome. J Clin Invest. 2004; 114:1752–1761. [PubMed: 15599400]
46. Anderson EJ, Yamazaki H, Neufer PD. Induction of endogenous uncoupling protein 3 suppresses mitochondrial oxidant emission during fatty acid-supported respiration. J Biol Chem. 2007; 282:31257–31266. [PubMed: 17761668]
47. Anderson EJ, et al. Mitochondrial H2O2 emission and cellular redox state link excess fat intake to insulin resistance in both rodents and humans. J Clin Invest. 2009; 119:573–581. [PubMed: 19188683]
48. Korshunov SS, Skulachev VP, Starkov AA. High protonic potential actuates a mechanism of production of reactive oxygen species in mitochondria. FEBS Lett. 1997; 416:15–18. [PubMed: 9369223]
49. Yu T, Robotham JL, Yoon Y. Increased production of reactive oxygen species in hyperglycemic conditions requires dynamic change of mitochondrial morphology. Proc Natl Acad Sci U S A. 2006; 103:2653–2658. [PubMed: 16477035]
50. Finck BN, et al. A potential link between muscle peroxisome proliferator- activated receptor-alpha signaling and obesity-related diabetes. Cell Metab. 2005; 1:133–144. [PubMed: 16054054]
51. Nawrocki AR, et al. Mice lacking adiponectin show decreased hepatic insulin sensitivity and reduced responsiveness to peroxisome proliferator-activated receptor gamma agonists. J Biol Chem. 2006; 281:2654–2660. [PubMed: 16326714]
52. Berglund ED, et al. Direct leptin action on POMC neurons regulates glucose homeostasis and hepatic insulin sensitivity in mice. J Clin Invest. 122:1000–1009. [PubMed: 22326958]
53. Livak KJ, Schmittgen TD. Analysis of relative gene expression data using real-time quantitative PCR and the 2(-Delta Delta C(T)) Method. Methods. 2001; 25:402–408. [PubMed: 11846609]
54. Scherer PE, Williams S, Fogliano M, Baldini G, Lodish HF. A novel serum protein similar to C1q, produced exclusively in adipocytes. J Biol Chem. 1995; 270:26746–26749. [PubMed: 7592907]
55. Combs TP, et al. A transgenic mouse with a deletion in the collagenous domain of adiponectin displays elevated circulating adiponectin and improved insulin sensitivity. Endocrinology. 2004; 145:367–383. [PubMed: 14576179]
56. Laplante M, et al. Tissue-specific postprandial clearance is the major determinant of PPARgamma-induced triglyceride lowering in the rat. Am J Physiol Regul Integr Comp Physiol. 2009; 296:R57–R66. [PubMed: 18971352]
57. Hultin M, Carneheim C, Rosenqvist K, Olivecrona T. Intravenous lipid emulsions: removal mechanisms as compared to chylomicrons. J Lipid Res. 1995; 36:2174–2184. [PubMed: 8576643]
58. Bligh EG, Dyer WJ. A rapid method of total lipid extraction and purification. Can J Biochem Physiol. 1959; 37:911–917. [PubMed: 13671378]
59. Seibler J, et al. Reversible gene knockdown in mice using a tight, inducible shRNA expression system. Nucleic Acids Res. 2007; 35:e54. [PubMed: 17376804]
60. Baer A, Bode J. Coping with kinetic and thermodynamic barriers: RMCE, an efficient strategy for the targeted integration of transgenes. Curr Opin Biotechnol. 2001; 12:473–480. [PubMed: 11604323]

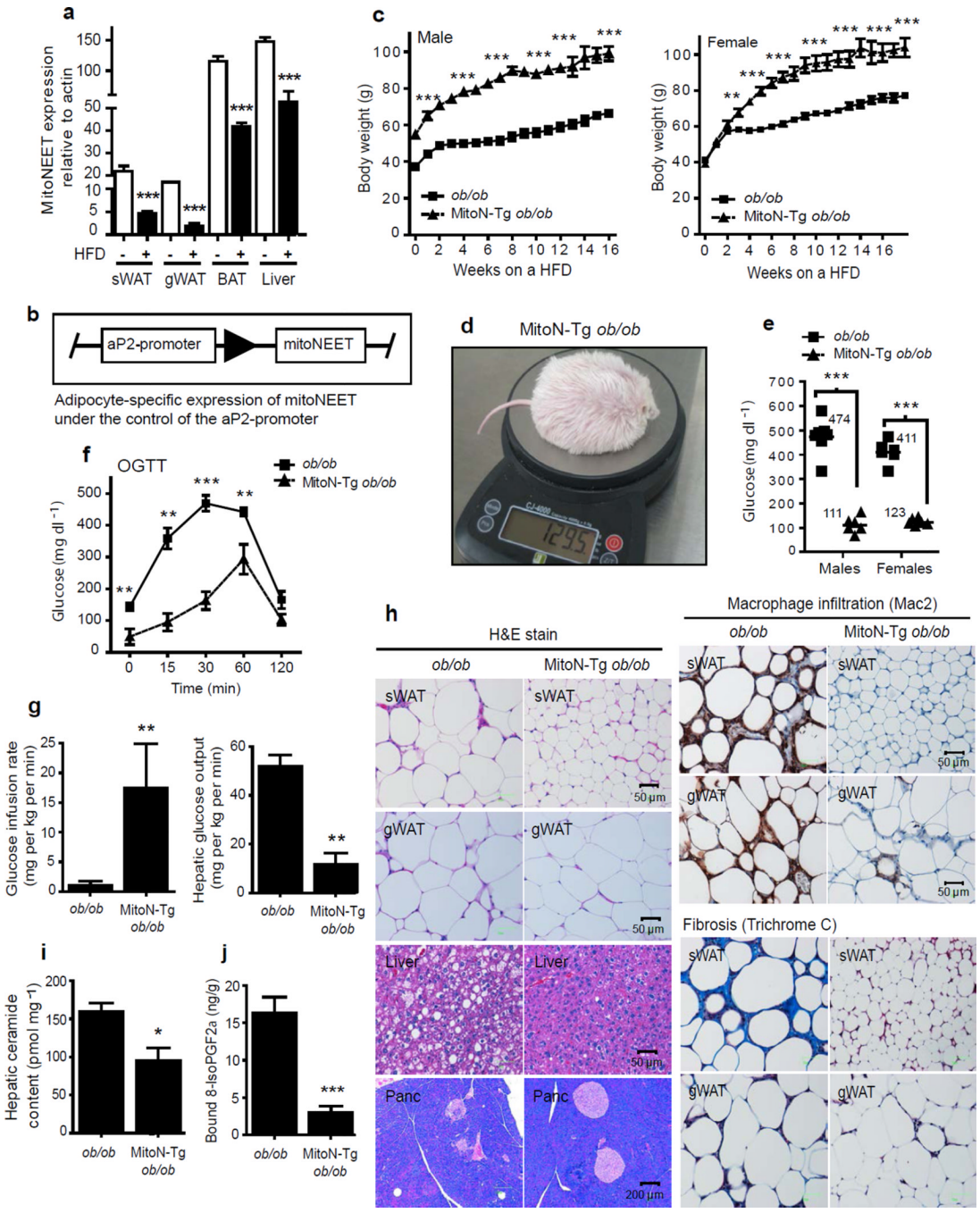

Figure 1.

MitoNEET causes massive AT expansion and improves hepatic insulin sensitivity. (**a**) MitoNEET levels in sWAT, gWAT, BAT and liver tissues from male FVB WT mice following 6-weeks of HFD feeding ($n = 4$ per group). (**b**) Schematic of the adipose-specific aP2-promoter-driven expression of mitoNEET. (**c**) Body-weights during HFD-feeding of male and female FVB *ob/ob* mice and MitoN-Tg *ob/ob* mice ($n = 6$ per group). (**d**) A photograph of the heaviest HFD-challenged MitoN-Tg FVB *ob/ob* female mouse to date. (**e**) Fed-state systemic glucose levels during HFD-feeding of FVB male and female *ob/ob* mice and MitoN-Tg *ob/ob* mice ($n = 6$ per group). (**f**) An OGTT (2.5 g kg^{-1} body-weight; single

gavage) on female FVB *ob/ob* and MitoN-Tg *ob/ob* mice ($n = 5$ per group). (**g**) Glucose infusion rates (left) and hepatic glucose output (right) during hyperinsulinemic-euglycemic clamps that were performed on conscious unrestrained 10 week-old female FVB *ob/ob* mice and MitoN-Tg *ob/ob* mice ($n = 5$ per group). (**h**) H&E staining (left), macrophage-infiltration (Mac2-immunohistochemistry) (top right) and fibrosis (Trichrome stain) (bottom right) of chow-fed FVB female *ob/ob* and MitoN-Tg *ob/ob* sWAT, gWAT, liver and pancreas, respectively. (**i**) Hepatic ceramide content in female FVB *ob/ob* mice and MitoN-Tg *ob/ob* mice ($n = 4$ per group). (**j**) Lipid-induced (15 ul g^{-1} body-weight 20% intralipid; single gavage) ROS-promoted lipid damage (lipid-peroxidation, as measured by bound 8-isoPGF2α levels) in FVB female *ob/ob* and MitoN-Tg *ob/ob* sWAT ($n = 5$ per group). $^{*}P < 0.05$; $^{**}P < 0.01$; $^{***}P < 0.001$.

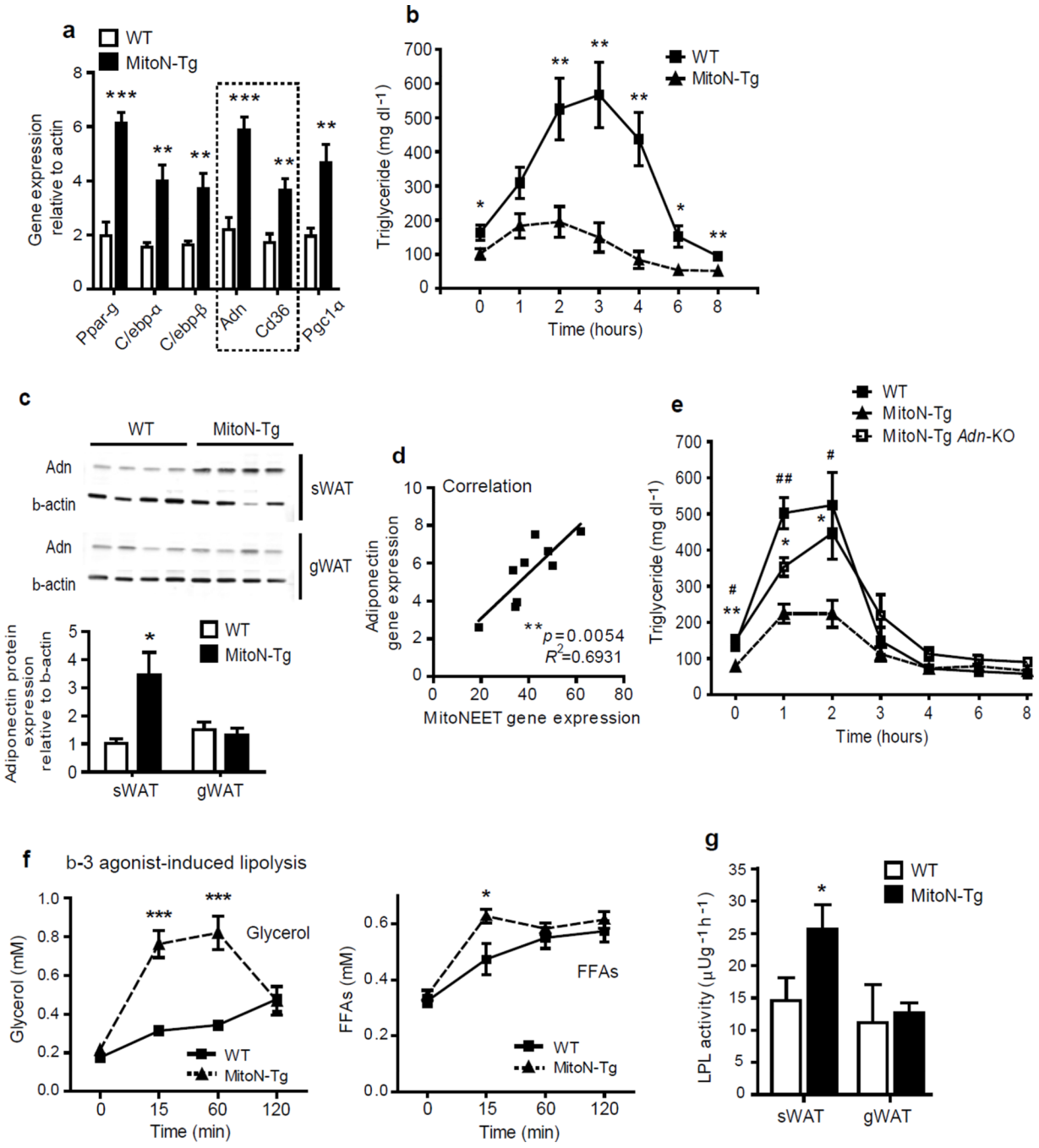

Figure 2.

MitoNEET promotes lipid-uptake by stimulating adiponectin production and heightening β-3 adrenergic agonist sensitivity. (**a**) RT-PCR showing gene expression levels of key microarray hits from male FVB WT versus MitoN-Tg sWAT ($n = 9$ per group). (**b**) TG clearance test (20% intralipid; 15 ul g^{-1} body-weight; single gavage) in male FVB WT versus MitoN-Tg mice ($n = 6$ per group). (**c**) Western blot demonstrating adiponectin expression in WT and MitoN-Tg sWAT and gWAT fat-pads ($n = 4$ per group). (**d**) The correlation between mitoNEET transgene levels and endogenous adiponectin message levels in MitoN-Tg sWAT ($n = 9$ per group). (**e**) TG clearance test (20% intralipid; 15 ul g^{-1} body-

weight; single gavage) in male FVB WT mice, MitoN-Tg mice and MitoN-Tg *Adn*-KO mice ($n = 6$ per group). (**f**) Circulating glycerol level (left) and FFA levels (right) in male FVB WT and MitoN-Tg mice during a β-3 adrenergic agonist sensitivity test (1 mg kg^{-1} CL316, 243 i.p., $n = 7$ per group). (**g**) LPL activity in WT and MitoN-Tg sWAT and gWAT ($n = 5$ per group).

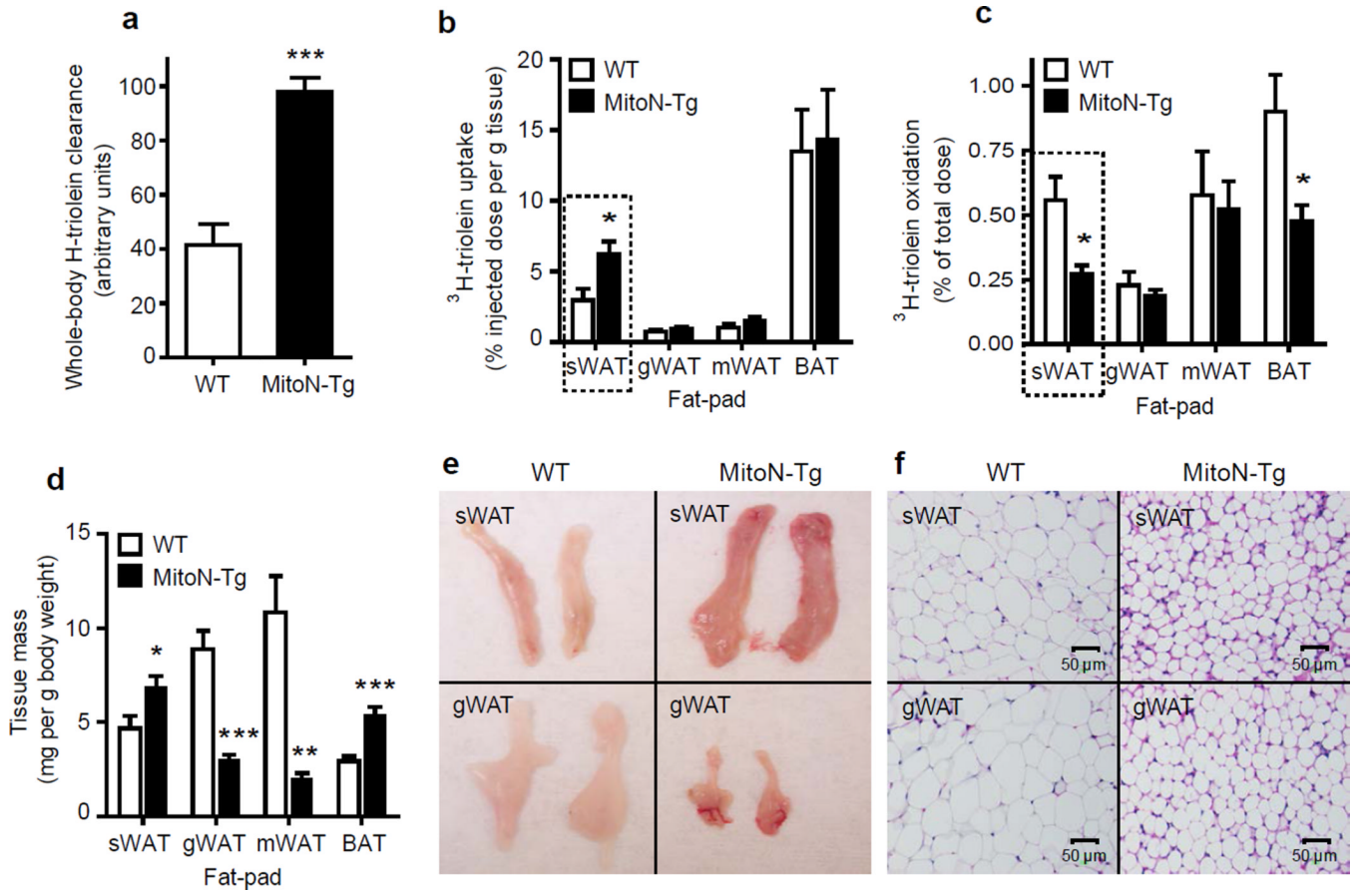

Figure 3.

MitoNEET induced alterations in fatty acid metabolism. (**a**) Whole-body ^{3}H-triolein lipid-clearance in male FVB WT mice versus MitoN-Tg mice, following 15 min post injection (2 µCi/mouse in 100 ul of 5% intralipid; single tail-vein injection) (n = 6 per group). (**b**) ^{3}H-triolein lipid-uptake, (**c**) β-oxidation and (**d**) tissue-mass in sWAT, gWAT, mWAT and BAT fat-pads of WT versus MitoN-Tg mice (n = 6 per group). (**e**) A representative photograph and (**f**) H&E staining of sWAT and gWAT fat-pads from a WT and MitoN-Tg mouse. *P < 0.05; **P < 0.01; ***P < 0.001.

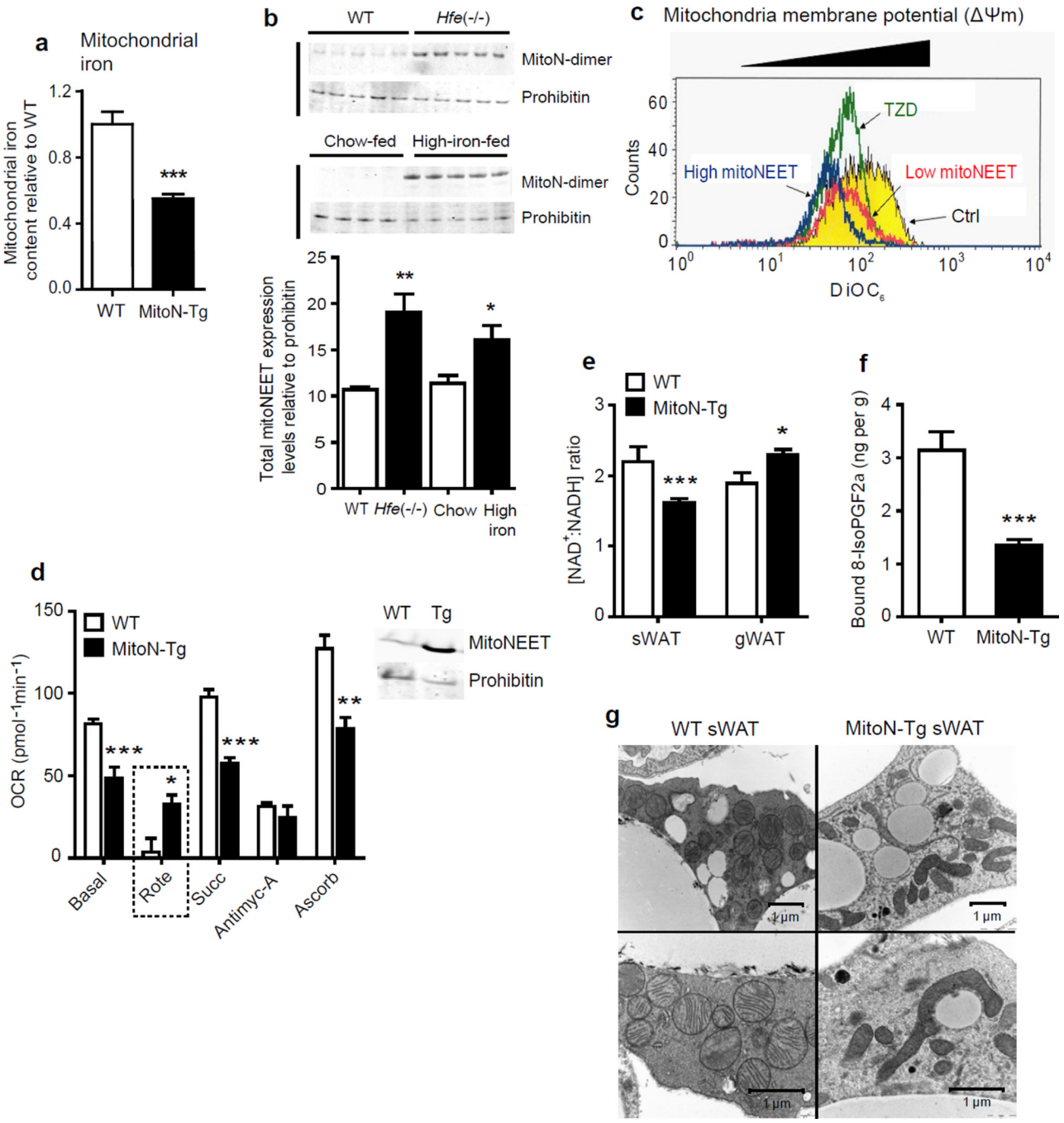

Figure 4.

MitoNEET compromises mitochondrial dynamics and morphology by modulating mitochondrial iron content. (**a**) Mitochondrial iron content in WT sWAT versus MitoN-Tg sWAT ($n = 7$ per group). ***$P < 0.001$. (**b**) Total mitoNEET expression levels (monomer and dimer) in WT mice versus H*fe*−/− mice (top panel), in addition to chow-fed control mice versus high iron-diet-fed ($n = 5$ per group). (**b**) Mitochondrial membrane potential (ΔΨm) using $DiOC_6$ incubated with control vehicle, or low- and high-mitoNEET expressing 3T3-L1 preadipocytes. Yellow-panel: control vehicle; green-panel: TZD-treated; red-panel: low mitoNEET expression; blue-panel: high mitoNEET expression. (**d**) Oxygen-

consumption rates (OCRs) in mitochondria (1 μg) isolated from WT (blue-panel) and MitoN-Tg (red-panel) sWAT, in response to sequential additions of DMEM (containing FCCP and, the substrates pyruvate and malate), rotenone (complex I inhibitor), succinate (complex II substrate), antimycin-A (complex III inhibitor), ascorbate and TMPD (cytochrome c substrate) ($n = 4$ per group). Prohibitin was utilized as a mitochondrial protein loading control. (**e**) NAD^+: NADH ratio in WT and MitoN-Tg sWAT and gWAT ($n = 5$ per group). (**f**) Lipid-induced (15 ul g^{-1} body-weight 20% intralipid; single gavage with tissues harvested following 6 h induction) ROS-promoted lipid damage (lipid-peroxidation, as measured by bound 8-isoPGF2α levels) in WT and MitoN-Tg sWAT ($n = 5$ per group). (**g**) Representative EM images (16,500× and 26,500× magnifications) of unchallenged WT and MitoN-Tg sWAT.

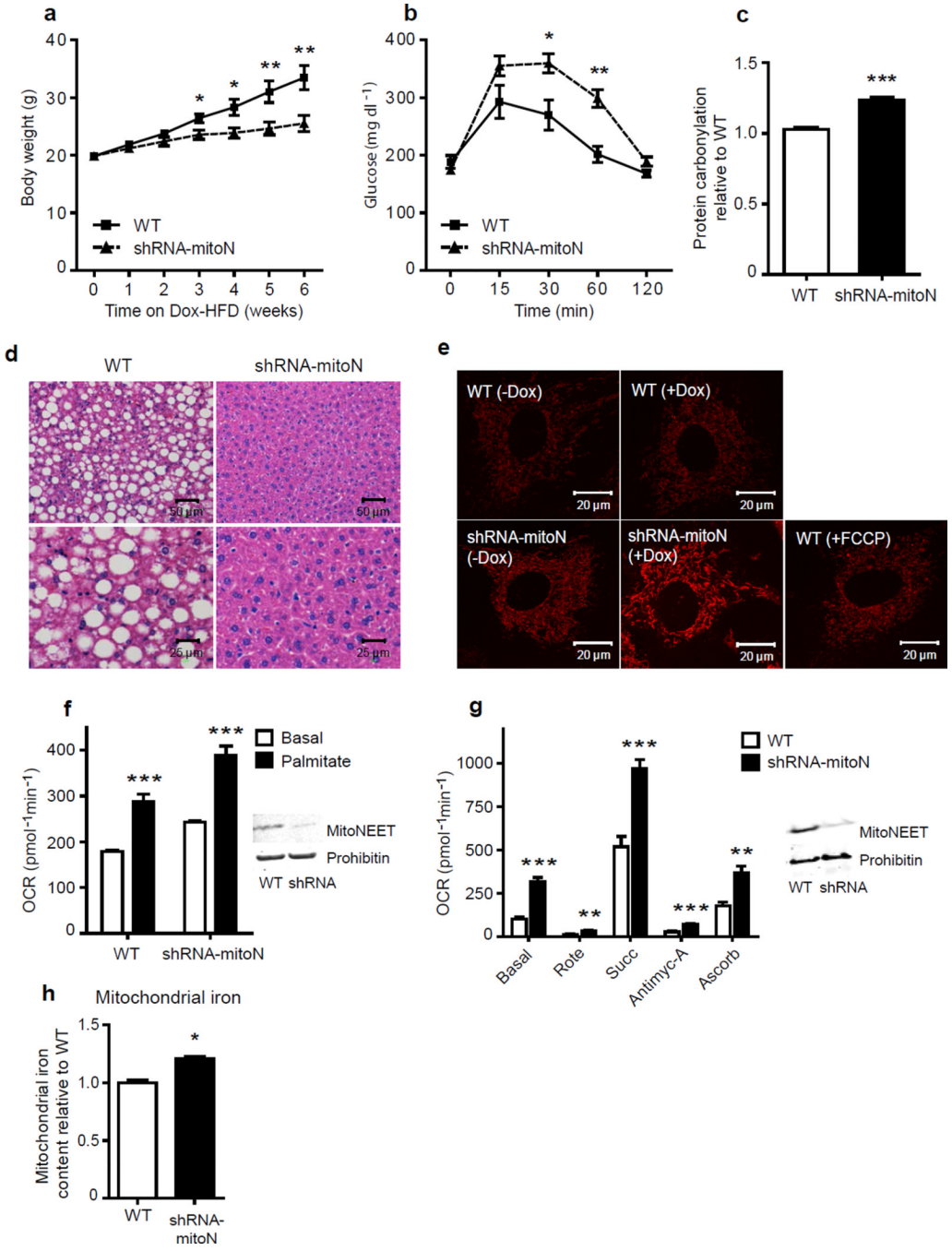

Figure 5.

A lack in mitoNEET enhances mitochondrial oxidative capacity. (**a**) Body-weight gain in male C57/BL6 WT and shRNA-mitoN mice during Dox-HFD feeding ($n = 5$ per group). (**b**) An OGTT (2.5 g kg^{-1} body-weight; single gavage) on male C57/BL6 WT and shRNA-mitoN mice following Dox-HFD-feeding ($n = 5$ per group). (**c**) Hepatic ROS-induced protein damage (protein carbonylation) in male C57/BL6 WT and shRNA-mitoN mice following Dox-HFD feeding ($n = 5$ per group). (**d**) Representative H&E staining of WT and shRNA-MitoN livers following Dox-HFD feeding. (**e**) TMRM-treated WT and shRNA-MitoN MEFs (with or without Dox-treatment) to assess $\Delta\Psi m$. The chemical uncoupler

FCCP was utilized as an additional control. All images were taken by confocal microscopy at 63× magnification. (**f**) OCRs in Dox-treated WT and shRNA-MitoN MEFs in response to basal-conditions (low glucose), followed by the addition of palmitate, then etomoxir (a carnitine palmitoyltransferase-1 inhibitor), to specify inhibition of CPT-1 dependent β-oxidation ($n = 10$ per group). (**g**) OCRs for mitochondria (5 μg) isolated from liver tissues from Dox-chow fed WT (blue-panel) and shRNA-MitoN (red-panel) mice, in response to sequential additions of DMEM (containing FCCP and the substrates pyruvate and malate), rotenone, succinate, antimycin-A, then ascorbate and TMPD ($n = 4$ per group). Prohibitin was used as a mitochondrial protein loading control. (**h**) Mitochondrial iron content in WT liver versus shRNA-mitoN liver ($n = 7$ per group). $^{*}P < 0.05$; $^{**}P < 0.01$; $^{***}P < 0.001$.

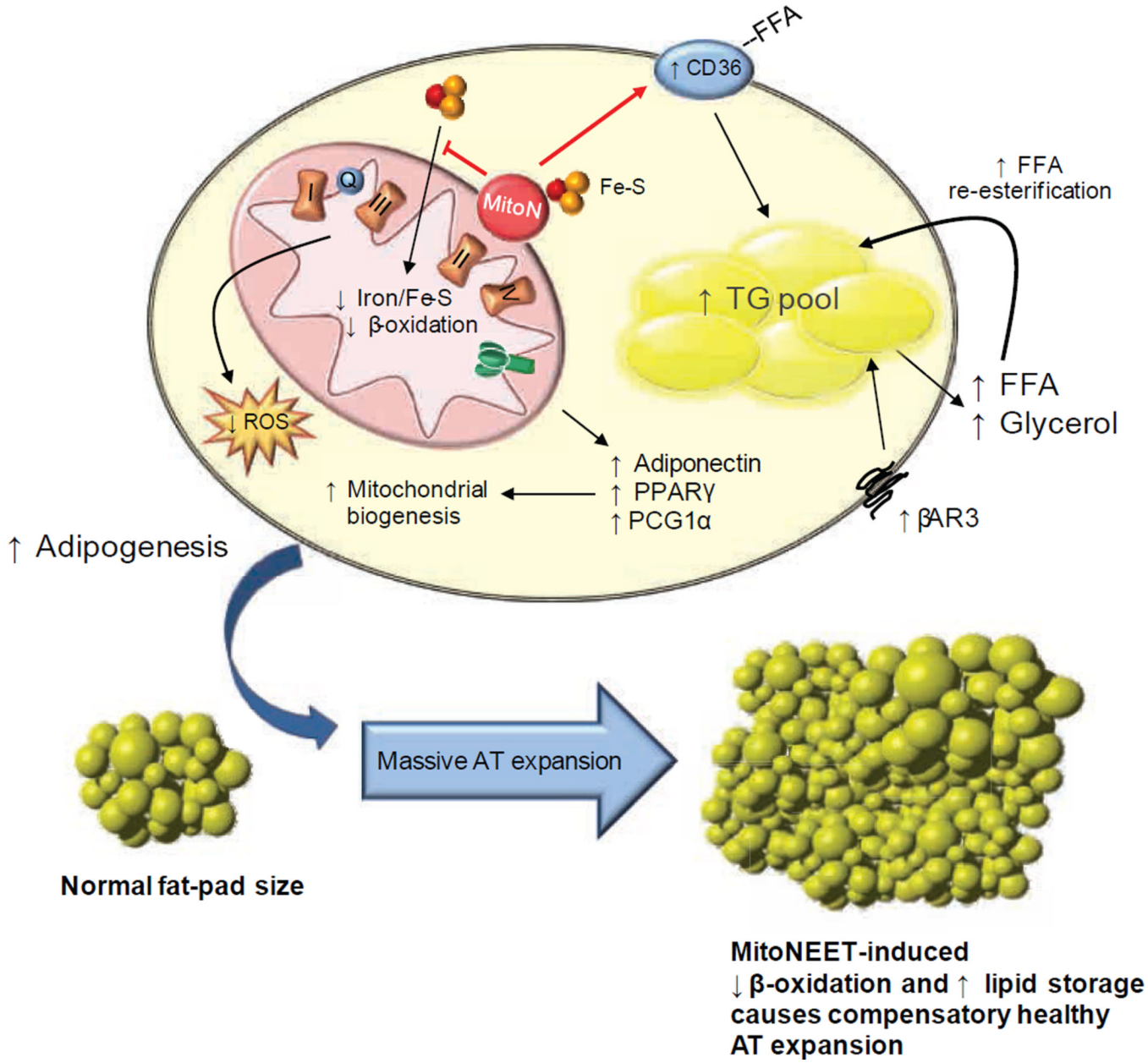

Figure 6. Proposed mechanism of mitoNEET action

Schematic representation of the intracellular involvement of mitoNEET in adipocyte physiology based on its ability to manipulate mitochondrial function. There are system-wide metabolic consequences arising from a mitoNEET-induced mitochondrial perturbation at the level of the adipocyte. MitoNEET i) impacts mitochondrial iron content, which may contribute to the decline in β-oxidation and, ii) enhances FA-uptake by signaling via Cd36. Compromised mitochondrial function therefore triggers a compensatory upregulation of adipogenesis, β-3 adrenergic signaling and mitochondrial biogenesis. The cellular decrease in mitochondrial activity further enhances lipid-influx into the cell. The inability to utilize these lipids effectively in mitochondria shunts surplus substrates into the TG pool. Consequently, low β-oxidation rates, high Ppar-γ activity accompanied by excess lipid storage, results in gross AT expansion. The ability to store massive amounts of lipids in

sWAT results in a highly beneficial system-wide improvement in whole-body insulin-sensitivity, with minimized lipotoxic effects in other tissues.